Journal of Alloys and Compounds 637 (2015) 98–105

Contents lists available at ScienceDirect

Journal of Alloys and Compounds

journal homepage: www.elsevier.com/locate/jalcom

Liquidus projection and isothermal section at 650 °C of ternary Co–Sb–Ga system

Sinn-wen Chen [a,*], Yuan-chun Chien [a], Wei-an Chen [a], Jui-shen Chang [a], Ssu-ming Tseng [a], G. Jeffrey Snyder [b]

[a] Department of Chemical Engineering, National Tsing Hua University, Taiwan
[b] Materials Science, California Institute of Technology, United States

ARTICLE INFO

Article history:
Received 27 November 2014
Received in revised form 8 February 2015
Accepted 25 February 2015
Available online 3 March 2015

Keywords:
Liquidus projection
Isothermal section
Thermoelectric material

ABSTRACT

Co–Sb–Ga ternary system is of interests for thermoelectric applications. Alloys quenched from completely molten state with compositions of the entire Co–Sb–Ga regime and alloys equilibrated at 650 °C with compositions in the $CoSb_3$–CoGa–Ga–Sb regime were prepared and analyzed. The liquidus projection and isothermal section at 650 °C of ternary Co–Sb–Ga system were determined based on these experimental results and the phase diagrams of its three constituent binary systems. The liquidus projection has 10 primary solidification phase regions. They are Co, CoSb, $CoSb_2$, $CoSb_3$, Sb, GaSb, Ga, $CoGa_3$, CoGa and a ternary compound, $Co_3Sb_2Ga_4$, which is newly found. There are three class I and six class II invariant reactions involving with liquid phase. Except for the L ↔ Co + CoSb + CoGa, L + CoGa ↔ $Co_3Sb_2Ga_4$ + GaSb reaction, the reaction temperatures are determined using DTA. In the $CoSb_3$–CoGa–Ga–Sb region, there are 5 tie-triangles, which are $CoSb_3$ + Liquid + GaSb, $Co_3Sb_2Ga_4$ + $CoSb_3$ + GaSb, CoGa + $Co_3Sb_2Ga_4$ + GaSb, CoGa + GaSb + $CoGa_3$, and $CoGa_3$ + GaSb + Liquid. The ternary solubilities in most of the binary compounds are not significant, and the highest is 3.5 at.% Sb in the CoGa.

1. Introduction

Thermoelectric materials have attracted very intensive research interests recently driven primarily by the needs of compact electronic cooling and especially for the power generation from waste heat [1–12]. $CoSb_3$ is a skutterudite compound. Skutterudite is a cubic structure with two cages per unit cell, and it is possible to incorporate atoms into cages [1]. It has been reported that $CoSb_3$-based filled skutterudites have promising thermoelectric properties [1–12]. Among various filling atoms, Ga has been found to be a very suitable candidate [9–12].

Phase equilibria knowledge is basic information, and is important for materials' development and properties' assessment [13,14]. Phase diagrams of the Co–Sb–Ga's constituent binary systems, Co–Sb, Co–Ga, and Ga–Sb, have been critically examined [15–20]. The crystal structures of related phases in these binary systems have been determined [16,18,19] and are summarized in Table 1. However, except for one isothermal section at 500 °C [21] and one about compound defect [12], there are no available phase equilibria literatures of the Co–Sb–Ga ternary system. In order to provide fundamental understanding of the Co–Sb–Ga ternary system which is important for thermoelectric applications, this study determines its liquidus projection and isothermal section at 650 °C.

2. Experimental procedures

Ternary Co–Sb–Ga alloys were prepared with pure Co foil (99.95%, Alfa Aesar®), Sb shots (99.9999%, Alfa Aesar®) and Ga shots (99.9%, Alfa Aesar®). Proper amounts of pure constituent elements were weighed and encapsulated in a quartz tube at 10^{-5} bar vacuum. The sample capsule was placed at 1000 °C for three days to ensure a complete mixing of the alloy. For the liquidus projection determination, the sample capsule was removed from the furnace and cooled in air. For the isothermal section determination, the sample capsules were quenched in water. The overall compositions of the alloys were carefully checked after solidification. No significant evaporation was observed, and the mass loss of each sample after preparation was less than 1%.

For the liquidus projection determination, the as-solidified alloy ingot was cut into two halves. For the isothermal section determination, the quenched alloy was equilibrated at 650 °C for 2 month, and then the alloy was also cut into two halves. One half was for powder X-ray diffraction analysis (XRD, Rigaku Ultima IV/ED2802 N, Japan) with Cu Kα radiation source, and the other half was metallographically examined. Microstructures were studied using Optical microscopy (Olympus, BH, Japan) and Scanning Electron Microscopy (SEM, Hitachi, s-2500, Japan). Compositions were determined by Electron Probe Microanalysis (EPMA, JOEL, JXA-8600SX, Japan). The spot size of the EPMA is smaller than the dimension

* Corresponding author. Fax: +886 3 5715408.
E-mail address: swchen@mx.nthu.edu.tw (S.-w. Chen).

http://dx.doi.org/10.1016/j.jallcom.2015.02.179
0925-8388/

Table 1
Crystal structure data of the Co–Sb, Co–Ga, and Ga–Sb systems.

Phase	Pearson symbol	Space group	Strukturbericht designation	Prototype	References
(α-Co)	cF4	Fm-3m	A1	Cu	[18]
(ε-Co)	hP2	$P6_3/mmc$	A3	Mg	[18]
CoSb	hP4	$P6_3/mmc$	$B8_1$	NiAs	[18]
$CoSb_2$	oP6	Pnnm	C18	$FeAs_2$	[18]
$CoSb_2$	mP12	$P2_1/c$	–	$CoSb_2$	[18]
$CoSb_3$	cI32	Im-3	$D0_2$	$CoAs_3$	[18]
CoGa	cP2	Pm-3m	B2	CsCl	[16]
$CoGa_3$	tP16	P-4n2	–	–	[16]
(Ga)	oS8	Cmca	All	Ga	[16]
GaSb	cF8	F-43m	B3	ZnS	[19]
(Sb)	hR2	R3-m	A7	As	[18]

of each phase, and the measurement accuracy was around 0.1%. Pure Co, Sb and Ga were chosen for ZAF correction to compute intensities of Co Kα, Sb Lα and Ga Kα to concentrations [22].

3. Results and discussions

3.1. Liquidus projection

Fifty-four Co–Sb–Ga ternary alloys were prepared. Their nominal compositions are listed in Table 2 and shown in Fig. 1(a). The primary solidification phase, i.e. the first phase precipitates from the liquid during solidification, is usually bigger in size and in the center of grains, and can be identified in the as-solidified microstructure. Since the liquidus projection boundary delineates regions of various primary solidification phases, the information of primary solidification phase determined from the as-solidified alloys can be used to construct the boundaries of the liquidus projection as shown in Figs. 1(a) and 1(b). It needs mentioning that the

Table 2
Primary solidification phases of ternary Co–Sb–Ga alloys.

Alloy No.	Nominal composition (at.%)			Primary phase	Alloy No.	Nominal composition (at.%)			Primary phase
	Co	Sb	Ga			Co	Sb	Ga	
1	75	15	10	Co	28	0	80	20	GaSb
2	75	5	20	Co	29	0	75	25	GaSb
3	70	5	25	Co	30	5	62.5	32.5	Gasb
4	65	25	10	CoSb	31	2	64	34	GaSb
5	50	45	5	CoSb	32	5	55	40	GaSb
6	50	40	10	CoSb	33	3	43.5	53.5	GaSb
7	50	35	15	CoSb	34	10	52.5	37.5	$Co_3Sb_2Ga_4$
8	50	30	20	CoSb	35	10	55	35	$Co_3Sb_2Ga_4$
9	30	40	30	CoSb	36	15	50	35	$Co_3Sb_2Ga_4$
10	30	50	20	CoSb	37	15	45	40	$Co_3Sb_2Ga_4$
11	25	75	0	CoSb	38	10	40	50	CoGa
12	20	80	0	CoSb	39	20	30	50	CoGa
13	20	75	5	CoSb	40	20	20	60	CoGa
14	20	70	10	CoSb	41	25	35	40	CoGa
15	20	65	15	CoSb	42	25	40	35	CoGa
16	20	60	20	CoSb	43	30	30	40	CoGa
17	20	50	30	CoSb	44	40	20	40	CoGa
18	18	81	1	CoSb	45	40	30	30	CoGa
19	15	82.5	2.5	$CoSb_2$	46	50	20	30	CoGa
20	15	77.5	7.5	$CoSb_2$	47	60	10	30	CoGa
21	15	75	10	$CoSb_2$	48	50	0	50	CoGa
22	15	65	20	$CoSb_2$	49	40	10	50	CoGa
23	10	90	0	$CoSb_2$	50	30	10	60	CoGa
24	10	85	5	$CoSb_2$	51	25	0	75	CoGa
25	1	94.5	4.5	$CoSb_3$	52	10	30	60	$CoGa_3$
26	4	78	18	$CoSb_3$	53	10	20	70	$CoGa_3$
27	10	60	30	$CoSb_3$	54	10	10	80	$CoGa_3$

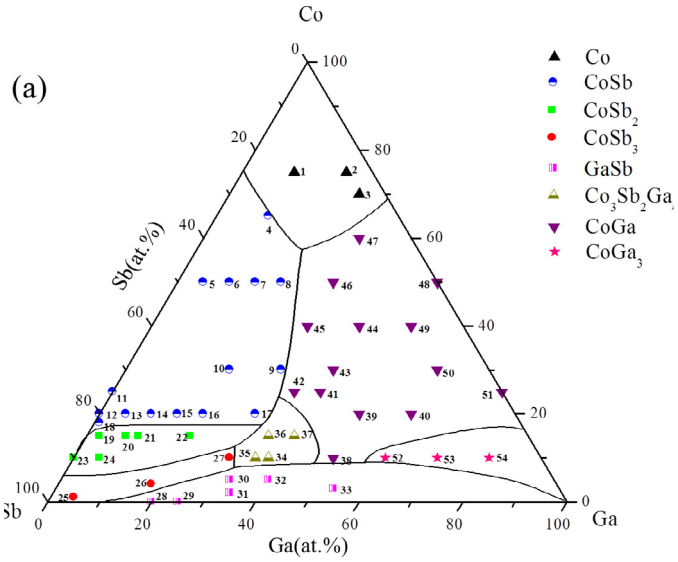

Fig. 1a. Compositions of ternary Co–Sb–Ga alloys examined in this study superimposed on the Co–Sb–Ga liquidus projection.

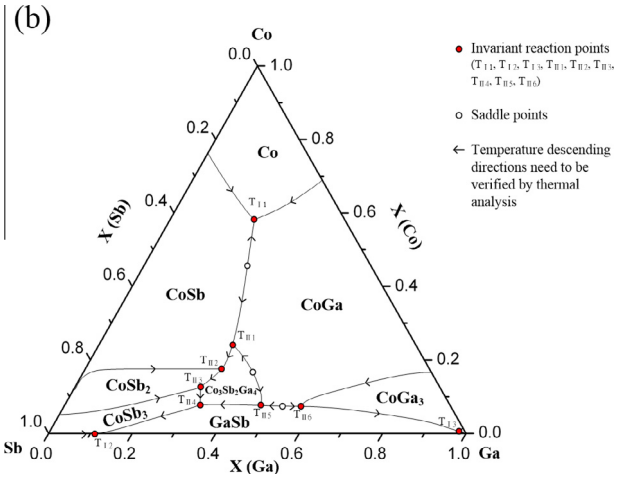

Fig. 1b. The Co–Sb–Ga liquidus projection.

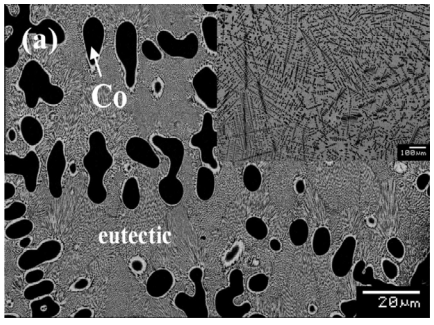

Fig. 2a. BSE micrograph of as-solidified alloy #1 displaying Co as its primary solidification phase.

reported compositions of alloys examined in this study are nominal results, and the compositions of specific phases are determined by EPMA.

Fig. 2(a) is the BSE (back-scattered electron image) micrograph of as-solidified alloy #1 (Co–15.0 at.% Sb–10.0 at.% Ga). The

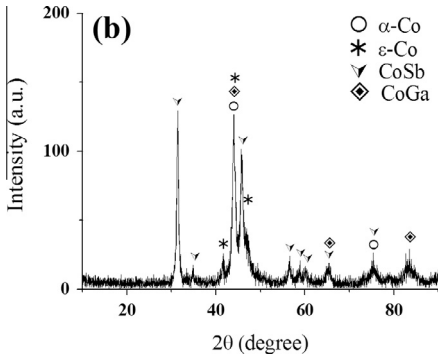

Fig. 2b. XRD diffractogram of as-solidified alloy #1.

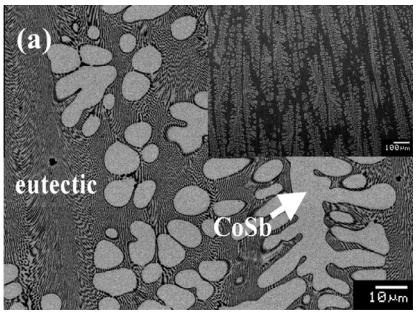

Fig. 3a. BSE micrograph of as-solidified alloy #4 displaying CoSb as its primary solidification phase.

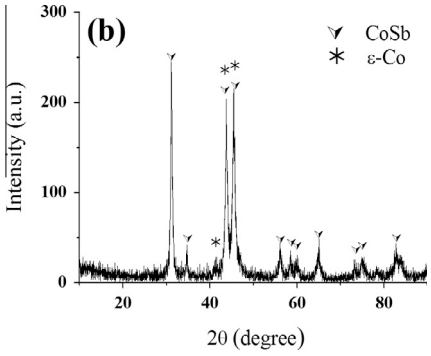

Fig. 3b. XRD diffractogram of as-solidified alloy #4.

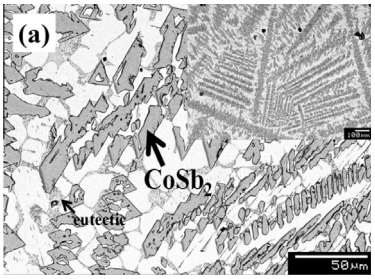

Fig. 4a. BSE micrograph of as-solidified alloy #19 displaying $CoSb_2$ as its primary solidification phase.

micrograph with lower magnification rate is superimposed on the upper-right corner. The dark dendritic phase is the primary solidification phase. Its composition is Co–1.2 at.% Sb–11.8 at.% Ga. Comparing with the available phase equilibria information

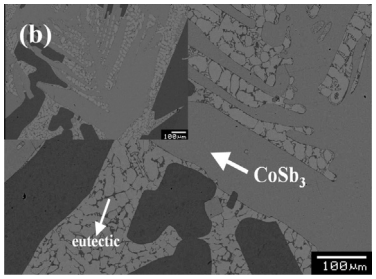

Fig. 4b. BSE micrograph of as-solidified alloy #26 displaying $CoSb_3$ as its primary solidification phase.

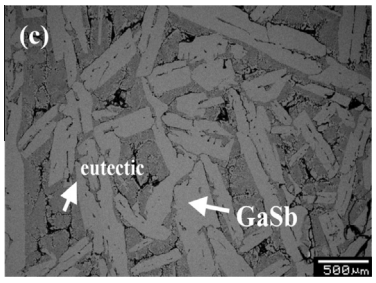

Fig. 4c. BSE micrograph of as-solidified alloy #33 displaying GaSb as its primary solidification phase.

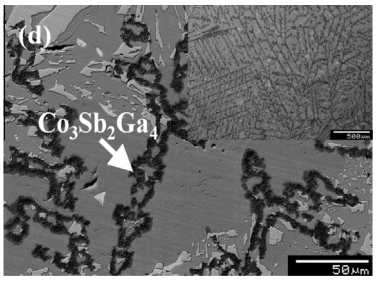

Fig. 4d. BSE micrograph of as-solidified alloy #37 displaying $Co_3Sb_2Ga_4$ as its primary solidification phase.

[15–21] and the phase equilibria determined in this study, the dark phase is the Co phase with Sb and significant Ga solubilities. Fig. 2(b) is its XRD diffractogram. Diffraction peaks of Co are observed and are consistent with EPMA determinations. These results indicate that the primary solidification phase of alloy #1 is the Co phase. Similar results are found for alloys #2 and #3, and their primary solidification phase is the Co phase.

Fig. 3(a) is the BSE micrograph of the as-solidified alloy #4 (Co–25.0 at.% Sb–10.0 at.% Ga). The primary solidification phase is the bright dendritic phase. Its composition is Co–34.4 at.% Sb–7.0 at.% Ga. Fig. 3(b) is the XRD diffractogram. Following similar procedures as mentioned above for alloys #1–#3, it is determined that the primary solidification phase of alloy #4 is the CoSb phase. Similar results are found in the alloys #5–#18. As summarized in Fig. 1(a) and Table 2, these total 15 alloys all have CoSb as their primary solidification phase.

Figs. 4(a)–4(f) are the BSE micrographs of the as-solidified alloys #19 (Co–82.5 at.% Sb–2.5 at.% Ga), #26 (Co–78.0 at.% Sb–18.0 at.% Ga), #33 (Co–43.5 at.% Sb–53.5 at.% Ga), #37 (Co–45.0 at.% Sb–40.0 at.% Ga), #39 (Co–30.0 at.% Sb–50.0 at.% Ga), and #52 (Co–30.0 at.% Sb–60.0 at.% Ga). Their primary solidification phases have been determined to be the $CoSb_2$, $CoSb_3$, GaSb,

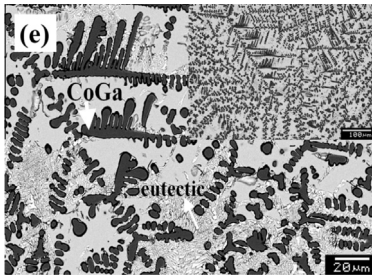

Fig. 4e. BSE micrograph of as-solidified alloy #39 displaying CoGa as its primary solidification phase.

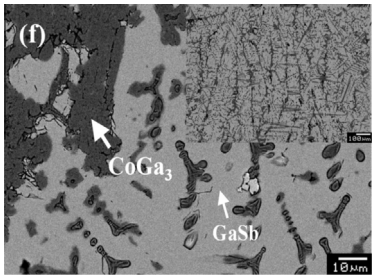

Fig. 4f. BSE micrograph of as-solidified alloy #52 displaying $CoGa_3$ as its primary solidification phase.

$Co_3Sb_2Ga_4$, CoGa and $CoGa_3$, respectively. This ternary $Co_3Sb_2Ga_4$ phase is a new compound and has not been reported previously [15–21]. It is going to be discussed in more details in Section 3.3.

The primary solidification phases of all the 54 alloys are determined and summarized in Table 2. Since the main purpose of this study is determination of the liquidus projection, the experimental efforts focus on the validation of the primary solidification phase and not the solidification path and other phases precipitated in later stages.

The experimentally determined results of primary solidification phases as mentioned above are used to construct the univariant lines of the Co–Sb–Ga liquidus projection. As shown in Figs. 1(a) and 1(b), the three sides of the ternary diagrams are binary and can be determined directly from the phase diagrams of its three binary constituent systems [15–20]. According to these phase diagrams [15–20], the primary solidification phases at the three sides from Co-corner counting counterclockwise are Co, CoSb, $CoSb_2$, $CoSb_3$, Sb, GaSb, Ga, $CoGa_3$ and CoGa phases. Similarly, the origins of these univariant lines along the three sides of the ternary triangles as shown in Figs. 1(a) and 1(b) can be determined from the binary phase diagrams as well [15–20], and are Co–25.4 at.% Sb, Co–89.2 at.% Sb, Co–95.3 at.% Sb, Co–~100 at.% Sb, Ga–88.2 at.% Sb, Ga–~0 at.% Sb, Co–~0 at.% Ga, Co–84.0 at.% Ga and Co–31.9 at.% Ga of the Co/CoSb, CoSb/$CoSb_2$, $CoSb_2$/$CoSb_3$, $CoSb_3$/Sb, Sb/GaSb, GaSb/Ga, Ga/$CoGa_3$, $CoGa_3$/CoGa and CoGa/Co boundaries, respectively. Together with the newly found ternary compound $Co_3Sb_2Ga_4$, there are ten primary solidification phases.

As shown in Fig. 1(b), there are nine ternary invariant reactions and the temperature descending directions of the univariant lines should be determined from thermal analysis. However, in most of the occasions, the liquid phase at the lower temperature is inside the tie-triangle of that at higher temperature, and thus the solidification path would follow the univariant line with lowering temperatures [23–25]. If it is assumed that the solidification path following the univariant lines, the temperatures descending directions could be derived from the mass balance requirements, i.e. the univariant lines move away from the solidified phases. For example, the Co/CoSb univariant line moves away Co–Sb side with the precipitations of Co and CoSb phases. According to the mass balance requirements, the temperature descending directions can be drawn as shown in Fig. 1(b), and there are three class I and six class II invariant reactions: $L \leftrightarrow Co + CoSb + CoGa$, $L \leftrightarrow CoSb_3 + Sb + GaSb$, $L \leftrightarrow Ga + CoGa_3 + GaSb$, $L + CoGa \leftrightarrow CoSb + Co_3Sb_2Ga_4$, $L + CoSb \leftrightarrow CoSb_2 + Co_3Sb_2Ga_4$, $L + CoSb_2 \leftrightarrow CoSb_3 + Co_3Sb_2Ga_4$, $L + Co_3Sb_2Ga_4 \leftrightarrow CoSb_3 + GaSb$, $L + CoGa \leftrightarrow GaSb + Co_3Sb_2Ga_4$ and $L + CoGa \leftrightarrow CoGa_3 + GaSb$.

It needs mentioning that not all the solidification paths follow the univariant lines of the liquidus projection. "Cross-over" phenomenon is observed in some systems [25], and thus some of the descending directions which are not confirmed with thermal analysis are marked with dash lines. The reaction temperatures

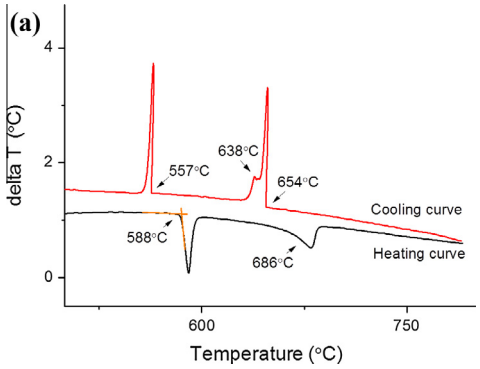

Fig. 5a. DTA heating and cooling curves of alloy #31.

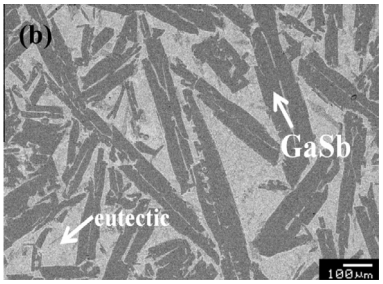

Fig. 5b. BSE micrograph of as-solidified alloy #31 displaying GaSb as its primary solidification phase.

were determined by using DTA (differential thermal analysis, DTA7, Perkin Elmer, U.S.A.). The procedures of DTA sample preparations and determinations of temperatures from DTA curves were mentioned previously [26–28]. The DTA curves at a 5 °C/min scanning rate and a BSE micrograph of as-solidified sample of alloy #31 (Co–64.0 at.% Sb–34.0 at.% Ga) are shown in Figs. 5(a) and 5(b). Three reaction peaks are observed in the cooling curve. According to the cooling curve and the proposed liquidus projection as shown in Fig. 1(b), the first peak of the highest reaction temperature at 654 °C is by the precipitation of GaSb, the second peak at 638 °C is by the monovariant reaction, and the third peak is caused by the class I reaction: $L \leftrightarrow CoSb_3 + Sb + GaSb$. Only two reaction peaks are found from the heating curve. As shown in the cooling curve, the temperatures of the two reactions at higher temperatures are near, and the reaction peaks might overlap in the heating curve and cannot be resolved. The reaction temperature of the first peak in the heating curve is at 686 °C and a significant undercooling of about 32 °C is observed. Due to the possible undercooling, the reaction temperatures are thus usually determined from the heating curves [26–28]. The reaction

Table 3
Invariant reactions in Co–Sb–Ga ternary system.

No.	Reaction	Temperature (°C)	Approximate composition Co:Sb:Ga (at.%)	Methods	References
T_{I1}	L ↔ Co + CoSb + CoGa	Not determined	52:28:20		
T_{I2}	L ↔ $CoSb_3$ + Sb + GaSb	588	0:88:12	DTA	This work
T_{I3}	L ↔ Ga + $CoGa_3$ + GaSb	29.77	1:1:98	Calculated	[18]
T_{II1}	L + CoGa ↔ CoSb + $Co_3Sb_2Ga_4$	818	25:44:31	DTA	This work
T_{II2}	L + CoSb ↔ $CoSb_2$ + $Co_3Sb_2Ga_4$	755	18:49:33	DTA	This work
T_{II3}	L + $CoSb_2$ ↔ $CoSb_3$ + $Co_3Sb_2Ga_4$	747	13:57:30	DTA	This work
T_{II4}	L + $Co_3Sb_2Ga_4$ ↔ $CoSb_3$ + GaSb	686	8:59:33	DTA	This work
T_{II5}	L + CoGa ↔ $Co_3Sb_2Ga_4$ + GaSb	Not determined	8:45:47		
T_{II6}	L + CoGa ↔ $CoGa_3$ + GaSb	687	7:36:57	DTA	This work

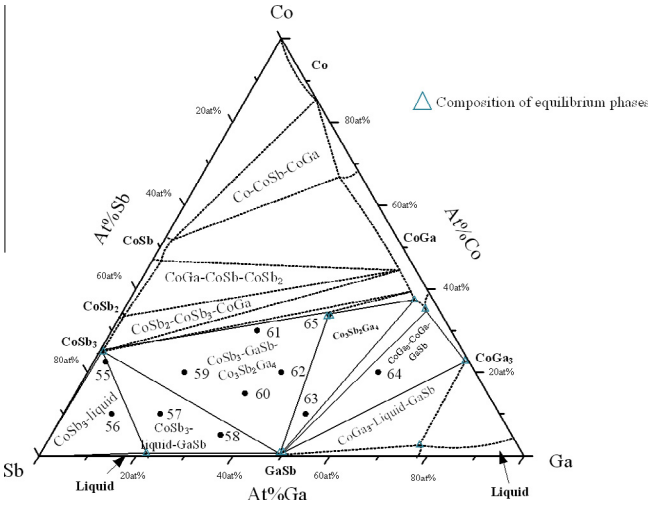

Fig. 6. Compositions of ternary Co–Sb–Ga alloys examined in this study superimposed on the Co–Sb–Ga 650 °C phase equilibria isothermal section.

temperature of L ↔ $CoSb_3$ + Sb + GaSb reaction is thus at 588 °C. Following similar procedures, the reaction temperatures were determined, and are summarized in Table 3.

3.2. Isothermal section of Co–Sb–Ga phase equilibria at 650 °C

Eleven Co–Sb–Ga ternary alloys were prepared and equilibrated at 650 °C. Their nominal compositions are superimposed in Fig. 6 and summarized in Table 4. Fig. 7(a) shows the BSE (back-scattered electron image) micrograph of alloy #57 (Co–70.0 at.% Sb–20.0 at.% Ga). Three phases are observed. The composition of the gray phase is Co–74.6 at.% Sb–0.4 at.% Ga, and it is $CoSb_3$ with 0.4 at.% Ga solubility. The composition of the dark phase is Sb–49.4 at.% Ga, and is GaSb phase with negligible Co solubility. The fine structure region contains various phases. Its average composition is Co–78.3 at.% Sb–20.9 at.% Ga and it was the liquid phase prior to its removal from the furnace. It needs mentioning that all the samples are analyzed at room temperature, and there is no liquid per se. The liquid phase mentioned in this study refers to the region which was liquid at the heat-treatment temperature. Fig. 7(b) is its XRD

Table 4
Equilibrium phases of Co–Sb–Ga alloys at 650 °C.

Alloy no.	Nominal composition Co:Sb:Ga (at.%)	The equilibrium phases formed in the alloys	Composition of phases by EPMA Co:Sb:Ga (at.%)	Equilibrated phases
55	22.5:75:2.5	$CoSb_3$ Liquid	24.8:74.6:0.6 0:86.6:13.4	$CoSb_3$ + liquid
56	10:80:10	$CoSb_3$ Liquid	24.2:75.2:0.6 0.1:87.5:12.4	$CoSb_3$ + liquid
57	10:70:20	$CoSb_3$ GaSb Liquid	25.0:74.6:0.4 0.1:50.6:49.4 0.8:78.3:20.9	$CoSb_3$ + liquid + GaSb
58	5:60:35	$CoSb_3$ Liquid GaSb	25.5:74.2:0.3 0.2:85.8:14.0 0:51.2:48.8	$CoSb_3$ + liquid + GaSb
59	20:60:20	$CoSb_3$ GaSb $Co_3Sb_2Ga_4$	25.2:74.2:0.6 0.2:50.7:49.1 33.7:23.8:42.5	$CoSb_3$ + GaSb + $Co_3Sb_2Ga_4$
60	15:50:35	$CoSb_3$ GaSb $Co_3Sb_2Ga_4$	24.8:74.6:0.6 0.4:51.1:48.5 33.8:23.7:42.5	$CoSb_3$ + GaSb + $Co_3Sb_2Ga_4$
61	30:40:30	$CoSb_3$ GaSb $Co_3Sb_2Ga_4$	25.8:73.7:0.6 1.0:49.9:49.1 33.9:23.2:42.9	$CoSb_3$ + GaSb + $Co_3Sb_2Ga_4$
62	20:40:40	$CoSb_3$ GaSb $Co_3Sb_2Ga_4$	25.3:74.1:0.6 0.3:50.0:49.7 32.9:23.3:43.8	$CoSb_3$ + GaSb + $Co_3Sb_2Ga_4$
63	10:40:50	CoGa GaSb $Co_3Sb_2Ga_4$	37.6:3.5:58.9 0.3:50.6:49.1 34.0:22.2:43.8	CoGa + GaSb + $Co_3Sb_2Ga_4$
64	20:20:60	$CoGa_3$ CoGa GaSb	22.9:0.1:77.0 25.0:2.4:62.6 0.4:49.8:49.8	$CoGa_3$ + CoGa + GaSb
65	34:23:43	$Co_3Sb_2Ga_4$	35.5:23.9:40.6	$Co_3Sb_2Ga_4$

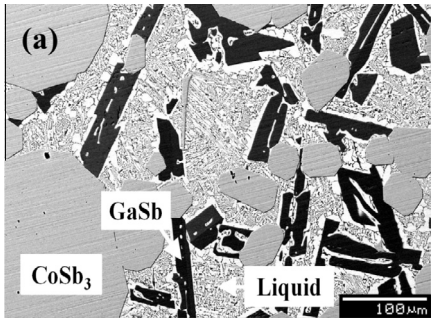

Fig. 7a. BSE micrograph of equilibrated alloy #57 displaying the existence of $CoSb_3$, GaSb, and liquid phases.

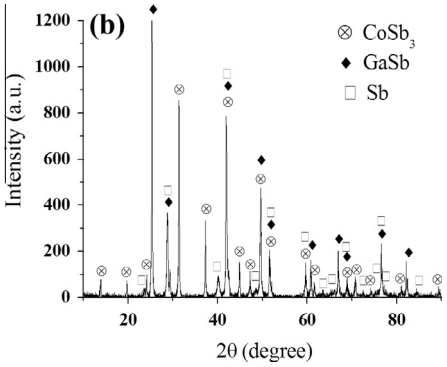

Fig. 7b. XRD diffractogram of equilibrated alloy #57.

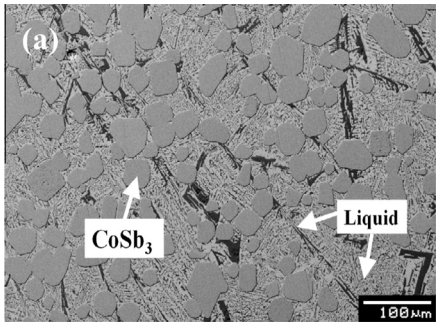

Fig. 8a. BSE micrograph of equilibrated alloy #56 displaying the existence of $CoSb_3$ and liquid phases.

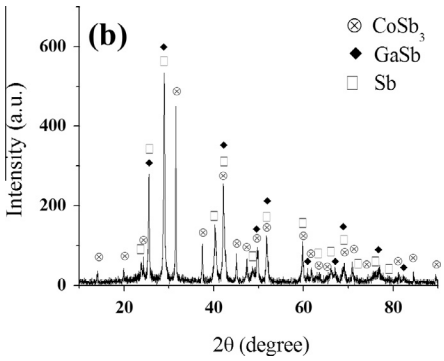

Fig. 8b. XRD diffractogram of equilibrated alloy #56.

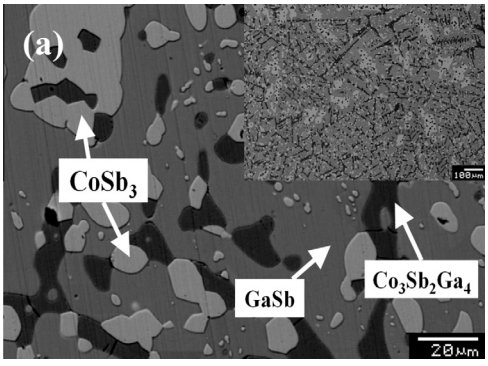

Fig. 9a. BSE micrograph of equilibrated alloy #60 displaying the existence of $CoSb_3$, $Co_3Sb_2Ga_4$, and GaSb phases.

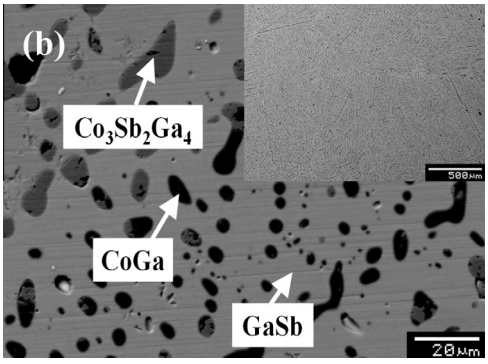

Fig. 9b. BSE micrograph of equilibrated alloy #63 displaying the existence of CoGa, $Co_3Sb_2Ga_4$, and GaSb phases.

diffractogram. Both the diffraction peaks of $CoSb_3$ and GaSb are observed, and Sb phase is formed during solidification. The microstructures and XRD analysis results indicate that the alloy #57 is located in $CoSb_3$ + liquid + GaSb three-phase region. Similar results are observed for alloy #58 (Co–60.0 at.% Sb–35.0 at.% Ga), and is in the $CoSb_3$ + liquid + GaSb three-phase region as well.

Fig. 8(a) is the BSE micrograph of alloy #56 (Co–80.0 at.% Sb–10.0 at.% Ga). Two phase regions are found. The composition of the gray phase is Co–75.2 at.% Sb–0.6 at.% Ga and is the $CoSb_3$. The average composition of the region with fine and dark dendritic phase is Co–87.5 at.% Sb–12.4 at.% Ga and was the liquid phase prior to its removal from the furnace. Fig. 8(b) is its XRD diffractogram. In addition to the $CoSb_3$ phase, the diffraction peaks of GaSb and Sb are observed and are formed during solidification. The results indicate that the alloy #56 is in the $CoSb_3$ + liquid two-phase region. Similar results are observed for alloy #55, and it is also in the $CoSb_3$ + liquid two-phase region.

Figs. 9(a)–9(d) are the BSE micrographs of alloys #60 (Co–50.0 at.% Sb–35.0 at.% Ga), #63 (Co–40.0 at.% Sb–50.0 at.% Ga), #64 (Co–20.0 at.% Sb–60.0 at.% Ga), and #65 (Co–23.0 at.% Sb–43.0 at.% Ga), respectively. They are in the $CoSb_3$ + GaSb + $Co_3Sb_2Ga_4$, CoGa + GaSb + $Co_3Sb_2Ga_4$, CoGa + $CoGa_3$ + GaSb and CoGa + $CoSb_3$ + $Co_3Sb_2Ga_4$ three-phase regions. The equilibrium phases formed in the alloys examined in this study are summarized in Table 4. The new ternary compound $Co_3Sb_2Ga_4$ has also been observed at 650 °C. It needs mentioning that ternary solubilities of the binary compounds are not significant, according to both the liquidus and isothermal section experiments in this study. The highest is 3.5 at.% Sb in the CoGa phase.

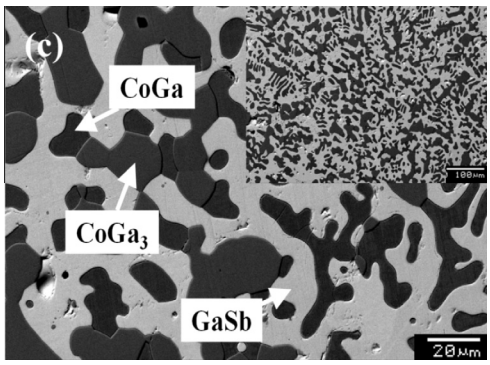

Fig. 9c. BSE micrograph of equilibrated alloy #64 displaying the existence of CoGa, $CoGa_3$, and GaSb phases.

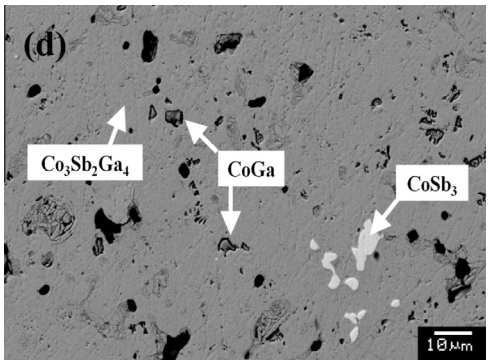

Fig. 9d. BSE micrograph of as-prepared alloy #65 displaying the existence of CoGa, $CoSb_3$, and $Co_3Sb_2Ga_4$ phases.

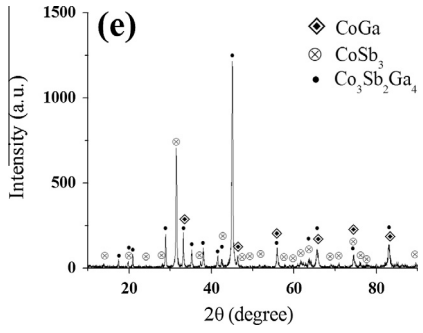

Fig. 9e. Powder X-ray diffractogram of alloy #65.

Since the three sides of the ternary phase diagram as shown in Fig. 6 are binary, the phase fields and the phase boundaries along the three sides of the Co–Sb–Ga tie-triangle can be determined from phase diagrams of its constituent binary systems [15–20]. At 650 °C, along the Co–Sb side, there are Co single phase region, Co + CoSb two-phase region, CoSb single phase region, CoSb + $CoSb_2$ two-phase region, $CoSb_2$ single phase region, $CoSb_2$ + $CoSb_3$ two-phase region, $CoSb_3$ single phase region, $CoSb_3$ + liquid two-phase region and liquid phase region. Similarly along the Sb–Ga and Ga–Co sides, there are liquid phase region, GaSb + liquid two-phase region, GaSb single phase region, GaSb + liquid two-phase region, liquid phase region, $CoGa_3$ + liquid two-phase region, $CoGa_3$ single phase region, CoGa + $CoGa_3$ two-phase region, CoGa single phase region, Co + CoGa two-phase region and Co single phase region.

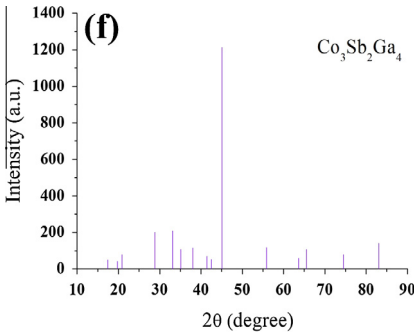

Fig. 9f. The derived X-ray diffractogram of $Co_3Sb_2Ga_4$.

Fig. 6 is the proposed 650 °C isothermal section based on the experimental results determined in this study of alloys in the $CoSb_3$–CoGa–Ga–Sb regime and the phase diagrams of the three constituent binary systems [15–19]. In addition to these single-phase and two-phase regions as mentioned above, the two-phase regions with the $Co_3Sb_2Ga_4$ compound are CoGa + $Co_3Sb_2Ga_4$, $Co_3Sb_2Ga_4$ + $CoSb_3$ and $Co_3Sb_2Ga_4$ + GaSb. The tie-triangles at 650 °C are Co + CoSb + CoGa, CoSb + $CoSb_3$ + CoGa, CoSb + $CoSb_2$ + $CoSb_3$, CoGa + $CoSb_3$ + $Co_3Sb_2Ga_4$, CoGa + $Co_3Sb_2Ga_4$ + GaSb, CoGa + GaSb + $CoGa_3$, $Co_3Sb_2Ga_4$ + $CoSb_3$ + GaSb, $CoSb_3$ + Liquid + GaSb and $CoGa_3$ + GaSb + Liquid. Since there are no experimental results in the Co–$CoSb_3$–CoGa region, the phase relationships in this region are proposed based on knowledge of phase equilibria and preliminary phase diagram calculation results and are marked with dashed lines.

It needs pointing out that only the $CoSb_3$–CoGa–Ga–Sb phase equilibria have been experimentally verified. The primary reason for the lacking of experimental data in the Co–$CoSb_3$–CoGa region is due to the experimental difficulties of very long annealing time required for the samples to reach equilibrium. Since there are no experimental results in the Co–$CoSb_3$–CoGa region, the phase relationships in this region are marked with dashed lines. These phase relationships need further verification by phase diagram calculation with rigorous thermodynamic modeling and more experimental determinations [29].

3.3. The ternary compound $Co_3Sb_2Ga_4$

Alloy # 65 (Co–23.0 at.% Sb–43.0 at.% Ga) was prepared following the alloy preparation procedures mentioned above, and then it was homogenized at 650 °C for 14 days. Fig. 9(d) is its BSE micrograph. Three phases are observed. The composition of the major gray phase is Co–23.9 at.% Sb–40.6 at.% Ga, and is the ternary compound $Co_3Sb_2Ga_4$. The dark phase is CoGa, and the bright phase is the $CoSb_3$. Although a pure $Co_3Sb_2Ga_4$ compound has not been prepared, the alloy #65 is composed of primarily the $Co_3Sb_2Ga_4$ compound as shown in Fig. 9(d). By extracting the diffraction peaks of CoGa and $CoSb_3$ phases, taking their relative intensities into consideration, from the XRD diffractogram of alloy #65 shown in Fig. 9(e), the diffraction peaks of this $Co_3Sb_2Ga_4$ phase can be derived as shown in Fig. 9(f). Since this phase has not been reported in the past, crystal structure's analysis is needed in the future and Fig. 9(f) is a valuable reference. It also needs mentioning that preliminary experimental results of the isothermal section of ternary Co–Sb–Ga system at 500 °C have also found this ternary compound $Co_3Sb_2Ga_4$.

4. Conclusion

A new ternary compound, $Co_3Sb_2Ga_4$, is found. It is a primary solidification phase and is stable at 650 °C. The ternary solubilities

in most of the binary compounds in ternary Co–Sb–Ga system are not significant. The liquidus projection has ten primary solidification phase regions. They are Co, CoSb, $CoSb_2$, $CoSb_3$, Sb, GaSb, Ga, $CoGa_3$, CoGa and $Co_3Sb_2Ga_4$ phases. The three class I and six class II reactions involving with liquid phase are L ↔ Co + CoSb + CoGa, L ↔ $CoSb_3$ + Sb + GaSb, L ↔ Ga + $CoGa_3$ + GaSb, L + CoGa ↔ CoSb + $Co_3Sb_2Ga_4$, L + CoSb ↔ $CoSb_2$ + $Co_3Sb_2Ga_4$, L + $CoSb_2$ ↔ $CoSb_3$ + $Co_3Sb_2Ga_4$, L + $Co_3Sb_2Ga_4$ ↔ $CoSb_3$ + GaSb, L + CoGa ↔ GaSb + $Co_3Sb_2Ga_4$, and L + CoGa ↔ $CoGa_3$ + GaSb. There are 9 tie-triangles in the 650 °C isothermal section. The 5 tie-triangles in the $CoSb_3$–CoGa–Ga–Sb region at 650 °C which have been experimentally verified are $CoSb_3$ + Liquid + GaSb, $Co_3Sb_2Ga_4$ + $CoSb_3$ + GaSb, CoGa + $Co_3Sb_2Ga_4$ + GaSb, CoGa + GaSb + $CoGa_3$ and $CoGa_3$ + GaSb + Liquid.

Acknowledgement

The authors acknowledge the financial support of National Science Council of Taiwan (NSC101-3113-P-008-001).

References

[1] Y. Kawaharada, K. Kurosaki, M. Uno, S. Yamanaka, Thermoelectric properties of $CoSb_3$, J. Alloys Comp. 315 (2001) 193–197.
[2] X.Y. Zhao, X. Shi, L.D. Chen, W.Q. Zhang, S.Q. Bai, Y.Z. Pei, X.Y. Li, T. Goto, Synthesis of $Yb_yCo_4Sb_{12}/Yb_2O_3$ composites and their thermoelectric properties, Appl. Phys. Lett. 89 (2006) 092121.
[3] T.M. Tritt, M.A. Subramanian, Thermoelectric materials, phenomena, and applications: a bird's eye view, MRS Bull. 31 (3) (2006) 188–198.
[4] Z. He, C. Stiewe, D. Platzek, G. Karpinski, E. Muller, S. Li, M. Toprak, M. Muhammed, Nano $ZrO_2/CoSb_3$ composites with improved thermoelectric figure of merit, Nanotechnology 18 (2007) 235602–235607.
[5] G.J. Snyder, E.S. Toberer, Complex thermoelectric materials, Nat. Mater. 7 (2008) 105–114.
[6] W.S. Liu, B.P. Zhang, L.D. Zhao, J.F. Li, Improvement of thermoelectric performance of $CoSb_{3-x}Te_x$ skutterudite compounds by additional substitution of IVB-group elements for Sb, Chem. Mater. 20 (2008) 7526–7531.
[7] A. Harnwunggmoung, K. Kurosaki, H. Muta, S. Yamanaka, High-temperature thermoelectric properties of thallium-filled skutterudites, Appl. Phys. Lett. 96 (20) (2010) 202107.
[8] P.X. Lu, F. Wu, H.L. Han, Q. Wang, Z.G. Shen, X. Hu, Thermoelectric properties of rare earths filled $CoSb_3$ based nanostructure skutterudite, J. Alloys Comp. 505 (2010) 255–258.
[9] Z. Xiong, X. Chen, X. Huang, S. Bai, L. Chen, High thermoelectric performance of $Yb_{0.26}Co_4Sb_{12}$/yGaSb nanocomposites originating from scattering electrons of low energy, Acta Mater. 58 (2010) 3995–4002.
[10] A. Harnwunggmoung, K. Kurosaki, T. Plirdpring, T. Sugahara, Y. Ohishi, H. Muta, S. Yamanaka, Thermoelectric properties of Ga-added $CoSb_3$ based skutterudites, J. Appl. Phys. 110 (2011) 013521.
[11] D. Zhao, H. Geng, X. Teng, Synthesis and thermoelectric properties of $Ga_xCo_4Sb_{11.7}Te_{0.3}$ skutterudites, Intermetallics 26 (2012) 31–35.
[12] Y. Qiu, L. Xi, X. Shi, P. Qiu, W. Zhang, L. Chen, J.R. Salvador, J.Y. Cho, Y. Yang, Y.C. Chien, S.W. Chen, Y. Tang, G.J. Snyder, Charge-compensated compound defects in Ga-containing thermoelectric skutterudites, Adv. Funct. Mater. 23 (2013) 3194–3203.
[13] F.N. Rhines, Phase Diagrams in Metallurgy: Their Development and Application, McGraw-Hill, New York, 1956.
[14] S.W. Chen, W. Gierlotka, H.J. Wu, S.K. Lin, Phase diagrams and their applications in Pb-free soldering, in: K.N. Subramanian (Ed.), Lead-Free Solders: Materials Reliability for Electronics, John Wiley & Sons Ltd., UK, 2012, pp. 13–44.
[15] A. Chari, A. Garay, R. Arroyave, Thermodynamic remodeling of the Co–Ga system, CALPHAD 34 (2010) 189–195.
[16] H. Okamoto, Co–Ga (cobalt–gallium), in: T.B. Massalski, H. Okamoto, P.R. Subramanian, L. Kacprzak (Eds.), Binary Alloy Phase Diagrams, ASM International, Ohio, 1990, pp. 1186–1189.
[17] K. Ishida, T. Nishizawa, The Co–Sb (cobalt–antimony) system, Bull. Alloy Phase Diagr. 11 (3) (1990) 243–248.
[18] Y. Zhang, C. Li, Z. Du, T. Geng, The thermodynamic assessment of the Co–Sb system, CALPHAD 32 (1) (2008) 56–63.
[19] T.L. Ngai, R.C. Sharma, Y.A. Chang, The Ga–Sb (gallium–antimony) system, Bull. Alloy Phase Diagr. 9 (1988) 586–591.
[20] I. Dervisevic, A. Todorovic, N. Talijan, J. Djokic, Experimental investigation and thermodynamic calculation of the Ga–Sb–Zn phase diagram, J. Mater. Sci. 45 (2010) 2725–2731.
[21] S.L. Markovski, J.A. van Beek, R.C.J. Schiepers, A.A. Kodentsov, F.J.J. van Loo, Thermodynamic evaluation of Ga–X–Co (X = P, As, Sb) systems related to the metallization of III–V compound semiconductors, J. Chim. Phys. 94 (1997) 992–997.
[22] P.E.J. Flewitt, R.K. Wild, Physical Methods for Materials Characterization, Institute of Physics Publishing, UK, Bristol and Philadelphia, 1994.
[23] O.F. Devereux, Topics in Metallurgical Thermodynamics, Krieger, Melbourne, Florida, 1983.
[24] S.W. Chen, J.S. Chang, K. Pan, C.M. Hsu, C.W. Hsu, Directional solidification and liquidus projection of Sn–Co–Cu system, Metall. Mater. Trans. A 44A (2013) 1656–1664.
[25] S.L. Chen, Y. Yang, S.W. Chen, X.G. Lu, Y.A. Chang, Solidification simulation using Scheil model in multicomponent systems, J. Phase Equilib. Diff. 30 (5) (2009) 429–434.
[26] S.W. Chen, C.C. Lin, C.M. Chen, Determination of the melting and solidification characteristics of solders using differential scanning calorimetry, Metall. Mater. Trans. A 29A (1998) 1965–1972.
[27] W.J. Boetinger, U.R. Kattner, K.-W. Moon, J.H. Perepezko, DTA and Heat-Flux DSC Measurements of Alloy Melting and Freezing, NIST, Washington, 2006.
[28] Y.C. Huang, S.W. Chen, K.S. Wu, Size and substrate effects upon undercooling of Pb-free solders, J. Electron. Mater. 39 (2010) 109–114.
[29] W. Gierlotka, S.W. Chen, W.A. Chen, J.S. Chang, G.J. Snyder, The Co–Sb–Ga System: Isoplethal Section and Thermodynamic Modeling, Metall. Mater. Trans. A 46 (4) (2015) 1488–1499.